Structure of the N Terminus of a Nonmuscle α-Tropomyosin in Complex with the C Terminus: Implications for Actin Binding[†,‡]

Norma J. Greenfield, Lucy Kotlyanskaya, and Sarah E. Hitchcock-DeGregori*

Department of Neuroscience and Cell Biology, Robert Wood Johnson Medical School, Piscataway, New Jersey 08854

Received October 1, 2008; Revised Manuscript Received December 10, 2008

ABSTRACT: Tropomyosin is a coiled-coil actin binding protein that stabilizes the filament, protects it from severing, and cooperatively regulates actin's interaction with myosin. Depending on the first coding exon, tropomyosins are low molecular weight (LMW), found in the cytoskeleton and predominant in transformed cells, or high molecular weight (HMW), found in muscle and nonmuscle cells. The N- and C-terminal ends form a complex that allows tropomyosin to associate N terminus-to-C terminus along the actin filament. We determined the structure of a LMW tropomyosin N-terminal model peptide complexed with a smooth/nonmuscle tropomyosin C-terminal peptide. Using NMR and circular dichroism we showed that both ends become more helical upon complex formation but that the C-terminal peptide is partially unfolded at 20 °C. The first five residues of the N terminus that are disordered in the free peptide are more helical and are part of the overlap complex. NMR data indicate residues 2−17 bind to the C terminus in the complex. The data support a model for the LMW overlap complex that is homologous to the striated muscle tropomyosin complex in which the ends are oriented in parallel N terminus-to-C terminus with the plane of the N-terminal coiled coil perpendicular to the plane of the C terminus. The main difference is that the overlap spans 16 residues in the LMW tropomyosin complex compared to 11 residues in the HMW striated muscle overlap complex. We discuss the relevance of a stable but dynamic intermolecular junction for high-affinity binding to actin.

A dynamic actin cytoskeleton is required for cellular movement, determination and maintenance of cellular shape, and numerous actin-dependent functions. The pleiotropic properties of the actin filament depend on its ability to bind a variety of proteins, many of which are the final targets in signaling pathways. In recent years tropomyosin has been recognized as the universal regulator of the actin filament (*1*).

Tropomyosins are encoded by a multigene family and are expressed in most eukaryotes in cell- and tissue-specific manners. In mammals there are four genes, with additional isoforms generated by alternative exon expression, by the use of alternate promoters and by formation of heterodimers (*1*). The alternate promoters result in two tropomyosin classes: high molecular weight (HMW)[1] tropomyosins that are ∼284 residues long and are expressed in both muscle and nonmuscle cells, and low molecular weight (LMW) tropomyosins (∼247 residues long) found in cellular cytoskeletons. In LMW tropomyosins the first exon, exon 1b, replaces exon 1a and 2 in the HMW tropomyosins. Although the sequences of the two classes of N-terminal ends are overall conserved within each class, relatively minor sequence differences can have a major effect on function (*2*). While much remains to be learned about the specific functions of nonmuscle tropomyosin isoforms, it has long been known that oncogenic transformation of cells is accompanied by downregulation of certain HMW tropomyosins (*1*).

The importance of the ends of tropomyosin for actin binding and regulatory function is well established. Both ends are encoded by alternatively expressed exons and are the binding sites for other proteins including tropomodulin at the N terminus (*3*) and troponin T in striated muscle isoforms (*4*). The extreme ends of striated muscle α-tropomyosin are required for cooperative binding to filamentous actin and Ca^{2+}-dependent regulation by troponin in muscle cells and

[†] This research was supported by NIH Grant GM-36326 to S.E.H.-D. and N.J.G., a grant from the UMDNJ Foundation to S.E.H.-D., and the Community Outreach program of the Northeast Structural Genomics Consortium (to Gaetano T. Montelione).

[‡] Coordinates of the structure of the N-terminal model peptide, $Tm1b_{1-19}Zip$, when bound to the C-terminal peptide, $TM9d_{252-284}$, have been deposited with the Protein Data Bank (PDB), http://www.rcsb.org/pdb/. The file accession number is 2k8x. The NMR data have been deposited with the BMRB (Biological Magnetic Resonance Data Bank), http://www.bmrb.wisc.edu/, accession number 15965.

* Corresponding author. E-mail: hitchcoc@umdnj.edu. Phone: 732-235-5236. Fax: 732-235-4029.

[1] Abbreviations: 1aNTD ($\alpha TM1a_{1-14}Zip$) and 1bNTD ($\alpha TM1b_{1-19}Zip$), model peptides containing residues 1−14 of rat striated muscle α-TM encoded by exon 1a or residues 1−19 of rat nonmuscle α-TM encoded by exon 1b, respectively, and the last 18 residues of GCN4 (both peptides have a glycine at the N terminus replacing the native acetyl group); 9aNTD ($\alpha TM9a_{251-284}$), a peptide containing residues 251−284 of rat striated α-striated muscle tropomyosin encoded by exon 8 and exon 9a with the sequence GCG at the N terminus to allow cross-linking; 9dCTD ($\alpha TM9d_{252-284}$), a peptide containing residues 252−284 of rat smooth and some nonmuscle α-tropomyosins encoded by exon 8 and exon 9d with the sequence GCGG at the N terminus to allow cross-linking. CD, circular dichroism; GCN4, a yeast transcription factor; HMW, high molecular weight; HSQC, heteronuclear single-quantum coherence; LWM, low molecular weight; NOE, nuclear Overhauser effect; NOESY, NOE spectroscopy; NOE cross-peaks, proton/proton interactions detected in nuclear Overhauser effect spectroscopy; rmsd, root-mean-square deviation; TM, tropomyosin.

10.1021/bi801861k CCC: $40.75
Published on Web 01/26/2009

modulate the cooperative interaction of myosin with the actin filament (*5, 6*).

The structures of isolated C- and N-terminal domains of tropomyosins have been solved in model peptides using NMR and X-ray crystallography (*7*−*12*). In the solution structure of the complex formed between the N- and C-terminal domains of rat striated muscle α-tropomyosin (1aNTD and 9aCTD, respectively) the chains of the C-terminal end spread apart to allow insertion of 11 residues of the N-terminal coiled coil into the resulting cleft (*13*). The structure of the C terminus in the complex is close to that found in crystal structures in which the chains form an antiparallel complex with another C-terminal molecule (*10, 12*). The 1aNTD in the complex is similar in structure to the uncomplexed peptide, but its chains are slightly spread apart (*7*).

In the 1aNTD/9aCTD complex, the plane of the N-terminal coiled coil is rotated 90° relative to the plane of the C terminus. A consequence of the geometry is that when the overlap complex is modeled into the X-ray structure of tropomyosin, the orientation of postulated periodic actin binding sites (*14*) on the coiled-coil surface is retained from one molecule to the next along the actin filament (*13*).

The LMW α-tropomyosins with exon 1b-encoded N termini bind with higher affinity to actin than HMW forms, despite being shorter, such that one molecule has only six instead of seven periodic repeats, the length of six actin subunits in the filament (*5*). The structure of the N terminus of unbound rat α-TM encoded by exon 1b was solved in a chimeric peptide, $\alpha TM1b_{1-19}Zip$ (1bNTD), using NMR (*9*). The main difference between the structures of $\alpha TM1a_{1-14}Zip$ (1aNTD) and 1bNTD is that exon 1b encodes an N-terminal extension of five residues that is disordered in the solution structure (*9*) and whose specific function is unknown.

Here we have used circular dichroism to analyze the affinity and folding properties of two peptides that model the intermolecular junction of short tropomyosins: 1bNTD, that contains residues encoded by exon 1b, and the C-terminal peptide, 9dCTD, that contains residues encoded by exon 9d. We determined the structure of 1bNTD in complex with the C terminus and the residues that interact with the C terminus using heteronuclear NMR and compared it to the structure of unbound 1bNTD. On the basis of the NMR results we propose a model for the nonmuscle complex in which the two peptides form a dynamic complex with a structure similar to but longer than that of striated muscle tropomyosin. We discuss the possible relevance to actin affinity of a stable complex that contains unfolded regions.

MATERIALS AND METHODS

Peptides. Unlabeled 1bNTD was synthesized at the Keck Facility at Yale University (New Haven, CT). Unlabeled $\alpha TM9a_{246-284}$ (9a39), $\alpha TM9d_{246-284}$ (9d39), $AcTM1a_{1-14}Zip$, and $GlyTM1a_{1-14}Zip$ were purchased from SynPep (Dublin, CA). 1bNTD labeled with ^{15}N or ^{15}N and ^{13}C was expressed and purified as previously described (*9*). Unlabeled 9dCTD was synthesized by the Tufts University Core Facility (Boston, MA). The peptide was cross-linked by disulfide formation catalyzed by the presence of $CuSO_4$ and K_3FeCN_6 (*15*). Oxidized and reduced peptides were separated using HPLC on a C18 reverse-phase column (Vydac 218TP10, Hesperia, CA). The concentrations of the peptides were determined using the microbiuret procedure of Goa (*16*). The peptides were dissolved in 0.01 mM sodium phosphate and 100 mM NaCl, pH 6.5, for all CD and NMR studies.

Circular Dichroism. Circular dichroism measurements were carried out as previously described (*2*). Data obtained as a function of temperature were fit to curves for the unfolding of monomers (CTD), dimers (NTD), and heterotrimers (NTD/CTD complex) (*17*). The helical contents of the peptides were determined using the program CDNN (*18*). To determine the binding constant of the 1bNTD/9dCTD complex, the 1bNTD peptide was titrated with a solution containing the same concentration of 1bNTD peptide and excess 9dCTD peptide to maintain constant 1bNTD concentration, as described by Greenfield (*19*). The binding constant was determined by the method of Engel (*20*) with a linear term to correct for the contribution of unbound 9dCTD. The combined equation is

$$y = M\{(1 + nkx + kP)/2kP - [((1 + nkx + kP)/2kP)^2 - nx/P]^{1/2}\} + mx + b$$

where y is the ellipticity as a function of total added 9dCTD, M is the maximal increase in ellipticity when 9dCTD binds to 1bNTD compared to the sum of the unmixed components, n is 1/number of binding sites, x is the total concentration of 9dCTD, k is the binding constant for the 1bNTD/9dCTD complex, P is the total concentration of 1bNTD, m is the change in ellipticity of unbound 9dCTD as a function of concentration, and b is the intercept of the unbound 9dCTD on the Y axis. Curve fitting using the Levenberg−Marquardt algorithm (*21*) was performed using SigmaPlot 8.0 (Systat Software, Inc., San Jose, CA), which was also used to create all the graphs in this paper.

Nuclear Magnetic Resonance. The NMR data were collected on a Varian Inova 600 spectrometer (Varian, Inc., Palo Alto, CA) equipped with a pulse-field gradient HCN cryoprobe. All measurements were performed in susceptibility-matched NMR tubes (Shigemi, Inc., Allison Park, PA). The sequential assignments and major structural studies were carried out at 20 °C, although HSQC and NOESY data of the complexes were also collected at 10 °C. Data processing and peak picking were performed as previously described (*13*). The chemical shifts of the C^{α} and C^{β} atoms of 1bNTD were only slightly changed by complex formation compared to those of unbound 1bNTD (*9*). Therefore, it was possible to determine the sequential assignments of the H^N, C^{α}, C^{β}, H^{α}, and H^{β} resonances using a minimal set of NMR experiments: $^{15}N-^{1}H$ HSQC (*22, 23*), HNCO (*24*), H(CA)(CO)NH, (CA)(CO)NH (*25, 26*), CBCA(CO)NH (*27*), and HBHA(CO)NH (*28*). The other side-chain resonances were determined using HCCH-COSY (*29, 30*) and $^{13}C-^{1}H$ HSQC (*22*) spectra.

Structure Determination. Distance constraints to determine the changes in structure of ^{13}C,^{15}N-labeled 1bNTD upon complex formation with unlabeled 9dCTD were obtained by analysis of ^{15}N-edited PFG NOESY-HSQC (*31*), ^{13}C-edited PFG NOESY-HSQC (*32*) and X-filtered ^{13}C-edited NOESY (*33*) experiments as previously described for uncomplexed 1bNTD and 9aCTD (*9, 11*) with the following modifications. To identify all interchain NOEs, a heterodimer of 1bNTD was prepared with one chain labeled with ^{15}N and ^{13}C and one chain unlabeled. The 1bNTD heterodimer was mixed

Table 1: Peptide Sequences

Peptide	Abbreviation	Sequence
N-terminal domain peptides		
αTM1a$_{1-14}$Zip[a]	(1aNTD)	gMDAIKKKMQMLKLDnyhlenevarlkklvger
αTM1b$_{1-19}$Zip[a,b]	(1bNTD)	gAGSSSLEAVRRKIRSLQEQnyhlenevarlkklvger
Heptad repeat		*a d a d a d a d a*
C-terminal domain peptides		
αTM9a$_{251-284}$[a,c]	(9aCTD)	gcgKSIDDLEDELYAQKLKYKAISEELDHALKDMTSI
αTM9d$_{252-284}$[a,d]	(9dCTD)	gcggSIDDLEEKVAHAKEENLSMHQMLDQTLLELNNM
αTM9a$_{246-284}$[c]	(9a39)	VTKLEKSIDDLEDELYAQKLKYKAISEELDHALKDMTSI
αTM9d$_{246-284}$	(9d39)	VTKLEKSIDDLEEKVAHAKEENLSMHQMLDQTLLELNNM
Heptad repeat		*a d a d a d a d a d a d*

[a] The residues which derive from tropomyosin are in upper case, and the residues from GCN4 or added to allow cross-linking are in lower case. [b] The first methionine residue encoded by exon 1b is cleaved following translation so the first residue in LMW tropomyosin is A1. [c] These peptides contain the mutation N279K, which increases peptide stability (*11*). [d] Residues 252−284 encoded by exon 9d in HMW rat α-TM correspond to residues 215−247 of rat LMW tropomyosins.

with unlabeled 9dCTD. X-filtered ^{13}C-edited NOESY cross-peaks from this complex are due to both intermolecular NOEs between the unlabeled 9d peptide and the labeled chain of the 1b peptide and intramolecular NOEs from the unlabeled to the labeled chain of the 1b peptide. To identify the intermolecular NOEs between the 9dCTD and 1bNTD, an X-filtered ^{13}C-edited NOESY experiment was performed in which both chains of the 9d peptide were unlabeled and both chains of the 1b peptide were labeled with ^{13}C and ^{15}N.

These intermolecular NOEs were removed from the data set obtained when only one chain of the 1bNTD peptide was labeled to identify the intramolecular−interchain cross-peaks. Only these were used for the structure determination of bound 1bNTD. The structure was calculated using AutoStructure v1.1.2 (*34, 35*), which calls DYANA (*36*) as a subroutine as previously described for the uncomplexed 1bNTD peptide (*9*). The structure was refined using CNS (*37*), as previously described (*13*).

Molecular Modeling. The 1bNTD/9dCTD complex was modeled on the structure of the complex of the striated muscle 1aNTD/9aCTD complex. First, the helical residues from 1aNTD (1−29) and 1bNTD (6−34) were aligned using the coordinates from model 1 of the 1aNTD/9aCTD complex (RCSB data bank 2g9j) and the coordinates from the first model of the 1bNTD structure in the presence of unlabeled 9dCTD determined herein. The residues were aligned using MOLMOL by removing the chain assignments and "TER" codes from the PDB files. The combined file was exported as a single PDB file. The coordinates of the 1aNTD were removed, the "TER" codes were added to separate the chains, and the hybrid 1bNTD/9aCTD molecule was imported into the program Sybyl v8.0 (Tripos International, St. Louis, MO). The coordinates from the 9aCTD (αTM$_{251-284}$) were changed to those of the 9dCTD (αTM$_{252-284}$), and the energy of the complex was minimized.

A molecular model of full-length LMW tropomyosin (LMW TM) was created based on model 1 of the X-ray structure of striated muscle tropomyosin (PDB code 1c1g (*38*),) using Sybyl v8.0. In LMW tropomyosins exon 1b, which encodes 44 residues, is expressed in place of exons 1a and 2 that encode residues 1−80 of HMW tropomyosins. The initial Met in the LMW rat α-tropomyosins (TM-5a and TM-5b (*39*)) is cleaved following translation; thus the first residue is A1. To model the N terminus encoded by exon 1b, residues 1−37 from chains A and B were deleted. Residues 38−80 were changed to residues 1−43 from rat TM-5a. To model the nonmuscle C terminus, residues 258−284 encoded by exon 9a were replaced by exon 9d-encoded residues, and the energy of the structure was minimized. To link two of the LMW TM models with the LMW overlap complex, the coordinates of residues 1−21 of the N terminus of one LMW TM model were replaced with those of the 1bNTD peptide complexed with the 9dCTD peptide, and the coordinates of the last 24 residues of a second LMW TM molecule were replaced with those from the model of the 9dCTD in the complex, as described previously for the 1aNTD/9aCTD complex (*13*).

RESULTS

Design of the Peptide Model System. The model system for determining the solution structure of the intermolecular junction between the ends of nonmuscle LMW tropomyosins is based on the model for the overlap region of striated muscle tropomyosin (Table 1) (*13*). The N-terminal domain peptide (1bNTD) is αTM1b$_{1-19}$Zip, the first 19 residues encoded by exon 1b followed by the last 18 residues of the leucine zipper region of the yeast transcription factor, GCN4 (*9*). The C-terminal domain peptide (9dCTD) is α-TM9d$_{252-284}$, the last 33 residues of the C terminus of smooth and nonmuscle α-tropomyosins in which residues 252−257 are those encoded by part of the constitutively expressed exon 8 and residues 258−284 by exon 9d (based on the residue

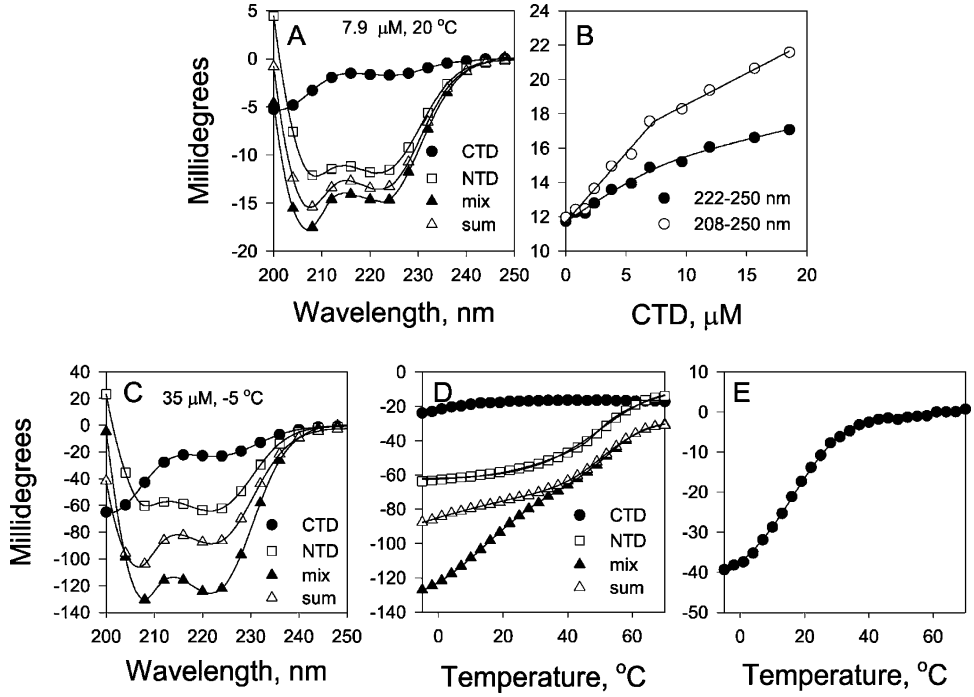

FIGURE 1: Dissociation constant and stability of the 1bNTD/9dCTD complex. (A) The ellipticity of (●) 9dCTD, 7.9 μM, (□) 1bNTD, 7.9 μM, (▲) a mixture of the 1bNTD and 9dCTD peptides, and (△) addition of the curves of the unmixed 1bNTD and 9dCTD peptides in 10 mM sodium phosphate and 100 mM NaCl, pH 6.5 at 20 °C. (B) Titration of 1bNTD, 7.9 μM, with increasing concentrations of 9dCTD plus 1bNTD, 7.9 μM at 20 °C: (○) 250−208 nm, (●) 250−222 nm. The data were not corrected for the contribution of unbound 9dCTD. The data were fit to a curve for the formation of a binary complex (*20*). (C) The ellipticity of (●) 9dCTD, 35 μM, (□) 1bNTD, 35 μM, (▲) a mixture of the 1bNTD and 9dCTD peptides, and (△) addition of the curves of the unmixed 1bNTD and 9dCTD peptides in 10 mM sodium phosphate and 100 mM NaCl, pH 6.5 at −5 °C. (D) The change in ellipticity as a function of temperature. Symbols and conditions are the same as in (C). The unfolding of 9dCTD is independent of protein concentration since it is cross-linked by a disulfide bond. (E) The ellipticity of the mixed 1bNTD and 9dCTD peptides minus the ellipticity of the individual peptides as a function of temperature. The unfolding data of 1bNTD and 9dCTD in (D) (all points) were fit by equations for the unfolding of a dimer and a monomer, respectively. The data in (D) and (E) for the unfolding of the 1bNTD/9dCTD complex were fit by curves for the unfolding of a monomer followed by the unfolding of a heterotrimer (*17*). Symbols show every eighth point in (A) and (C), all points in (B), every 15th point in (D), and every 10th point in (E). The data in (A) and (C) were smoothed (*63*).

numbering of a HMW, 284-residue TM). The addition of GCGG at the N terminus allows oxidative cross-linking of the peptide.

The C- and N-Terminal Domains of Short Tropomyosins Form a Stable Complex, but the C-Terminal Domain in the Complex Is Partially Disordered. Figure 1A shows the circular dichroism spectra of the 1bNTD and 9dCTD peptides, a mixture of the two peptides, and addition of the individual curves. At 20 °C the 1bNTD is ∼65% helical, but the 9d peptide is only ∼15% helical. Although it is mainly unfolded at 20 °C, the 9dCTD peptide binds tightly to the 1bNTD, and the binding is accompanied by a large increase in helical content. A one-to-one mixture of the peptides has a helical content of 43%, while addition of the curves for the 1bNTD and 9dCTD would give a helical content of only 33%. The increase in helical content upon binding was used to determine the dissociation constant of the 1bNTD/9dCTD complex (see Materials and Methods). When 1bNTD, 7.9 μM, was titrated with 9dCTD at 20 °C (Figure 1B), the ellipticity saturated at a 0.94 ± 0.03 molar ratio, indicating formation of a 1:1 complex with a K_d of <0.5 μM, too tight to measure accurately at the concentration used for the CD measurements.

Even though the binding is tight at 20 °C, the complex is not fully folded at this temperature. Figure 1C shows the spectra of the mixed and unmixed 1bNTD and 9dCTD peptides, 35 μM, at −5 °C. The helical content of 1bNTD is 75% helical, consistent with the solution structure (*9*). The helical content of the unbound 9dCTD is ∼25%, and it unfolds with a T_M of <0 °C (Figure 1D). The helical content of the 1:1 mixture is 73%, higher than that calculated for the addition of the spectra of the unbound peptides (∼50%) indicating binding. The unfolding and dissociation of the 1bNTD/9dCTD complex are not cooperative (Figure 1D,E). The complex begins to unfold before the chains dissociate. The major T_M of unfolding of the 1bNTD/1dCTD complex is 14.7 °C (Figure 1E), but this unfolding transition is independent of peptide concentration, suggesting that it does not represent dissociation of the NTD/CTD complex. In contrast, the 9aCTD is greater than 75% helical at 10 °C and unfolds with a T_M of ∼25 °C (*11*), and the unfolding and chain dissociation of complexes containing the exon 9a-encoded C terminus are cooperative.

The low stability of the exon 9d-encoded sequence is well established from studies of full-length tropomyosins and other model TM peptides (*6, 40, 41*). Moreover, it has been shown by comparing differential scanning calorimetry and CD that unfolding is noncooperative in full-length tropomyosins containing the N terminus encoded by exon 1b and the C terminus encoded by exon 9d (*42*), with substantial unfolding occurring without chain dissociation.

Noncooperative unfolding and dissociation of the complex of the C- and N-terminal domains of the nonmuscle short tropomyosin were also observed in another peptide model

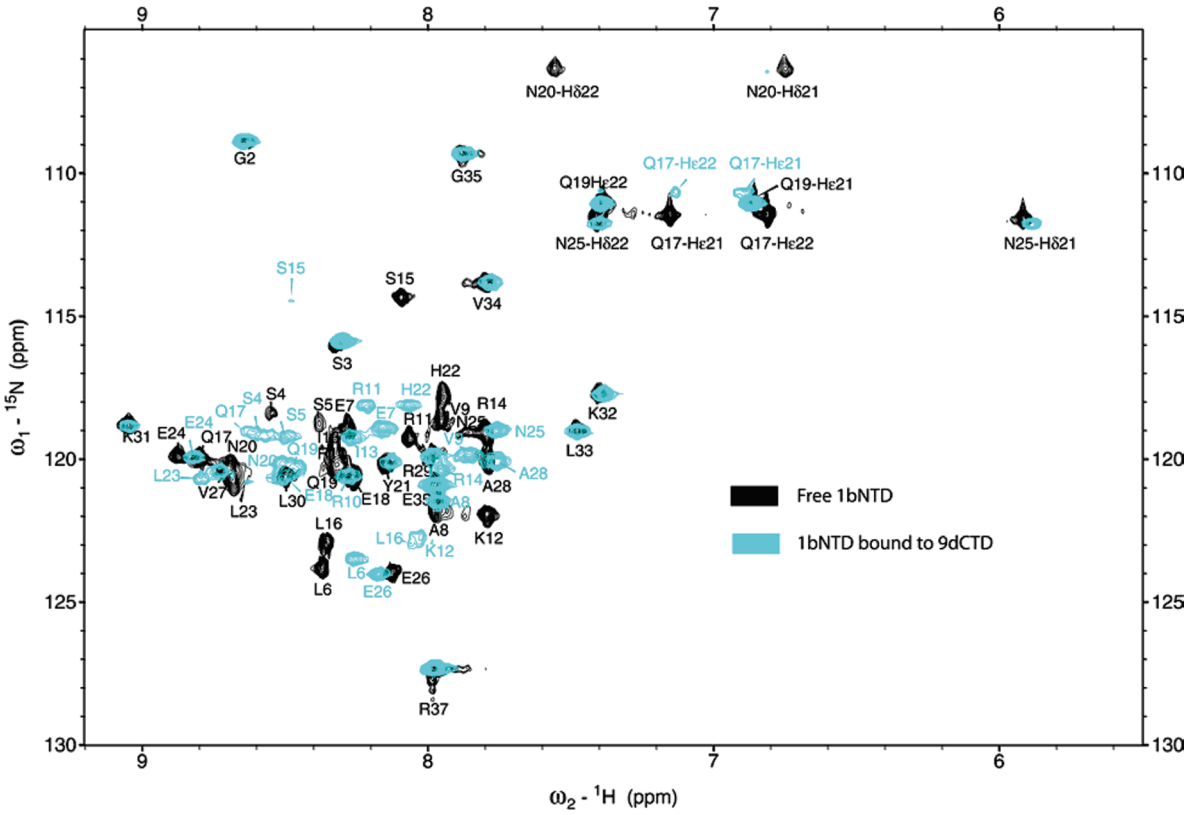

FIGURE 2: $^{15}N-^{1}H$ HSQC spectra of ^{15}N-1bNTD in the absence (black) and presence (cyan) of unlabeled 9dCTD at 20 °C. The cross-peaks from the free ^{15}N-1bNTD peptide are labeled in black. The cross-peaks from the peptide complex are labeled in cyan when they are displaced from those of the free peptide. The peptides were 0.35 mM in 100 mM NaCl and 10 mM sodium phosphate, pH 6.5. There is only one set of cross-peaks for both the free and complexed 1bNTD showing that the complex is symmetric.

for the exon 9d-encoded C terminus (*6*), described in Supporting Information, Figure S1. On the basis of the results with both peptides we conclude that the C terminus encoded by exon 9d binds with high affinity to the N terminus encoded by exon 1b but that the complexes begin to unfold and lose helical content before the chains dissociate. At 20 °C, the temperature used for determination of the solution structure, the two peptides bind tightly to each other, but extensive regions of the bound 9dCTD are disordered.

The $^{15}N-^{1}H$ HSQC Spectra of 1bNTD in Complex with 9dCTD. The $^{15}N-^{1}H$ HSQC spectra of $^{15}N^{13}C$-1bNTD or ^{15}N-1bNTD in complex with 9dCTD allowed initial characterization of the 1bNTD structure in the complex. Spectra were collected at 10, 15, and 20 °C. Many resonances were broadened at the lower two temperatures, but at 20 °C, all of the resonances were visible although some overlapped (Figure 2). There is only one set of resonances for all of the NH cross-peaks showing that the intermolecular junction is symmetric, as is the striated muscle 1aNTD/9aCTD complex (*13*).

The changes in chemical shifts and relative intensities of the cross-peaks of homologous residues of the 1aNTD and 1bNTD peptides differ in the two complexes (Figure 3). When 1bCTD was in a complex with 9dCTD, most of the cross-peaks near the N terminus gained in relative intensity, whereas those near the center of the molecule shifted (Figure 3A) and were broadened (Figure 3B). The H^N resonances from residues 14−17 in the $^{15}N-^{1}H$ HSQC spectra of 1bNTD were the most broadened upon complex formation with 9dCTD. A similar pattern of broadening was noted at 10 °C, but the relative broadening of residues 12−17 was more severe at the lower temperatures. Residues 6−36 of unbound 1bNTD are fully helical and have similar heteronuclear $^{1}H-^{15}N$ HNOE ratios and stabilities (*9*). The secondary structure of these residues does not change upon complex formation (see below). Therefore, the source of the exchange broadening of the resonances from residues 14−17 of 1bNTD most likely arises from their interactions with residues from the C terminus of the 9dCTD peptide undergoing chemical exchange between multiple conformations. The HSQC data are consistent with the CD results that show the bound 9dCTD peptide is partially unfolded at 20 °C.

The changes in the 1bNTD cross-peaks upon binding 9dCTD contrast with those of 1aNTD in complex with 9aCTD. The changes in the chemical shifts of homologous residues of ^{15}N-1bNTD are much larger than those of 1aNTD upon complex formation (Figure 3C,D; residue 1 of 1aNTD is homologous to residue 6 of 1bNTD). In addition, the relative intensities of all cross-peaks in the 1aNTD HSQC spectrum from the helical residues are similar although lower than those of the uncomplexed peptide. This suggests the broadening is due to slower tumbling of the entire molecule upon complex formation, rather than exchange broadening. The lack of exchange broadening of the 1aNTD spectrum upon complex formation with the 9aCTD is consistent with the small changes in the T1, T2, and HNOE data of the 1aNTD in complex with the 9aCTD previously reported (*10*), which show that most of the NTD residues in the 1a9a complex are ordered and have similar HNOEs and relaxation rates.

The Secondary Structure of $^{15}N^{13}C$-1bNTD Complexed with Unlabeled 9dCTD. The H^{α}, H^N, C^{α}, and C′ chemical

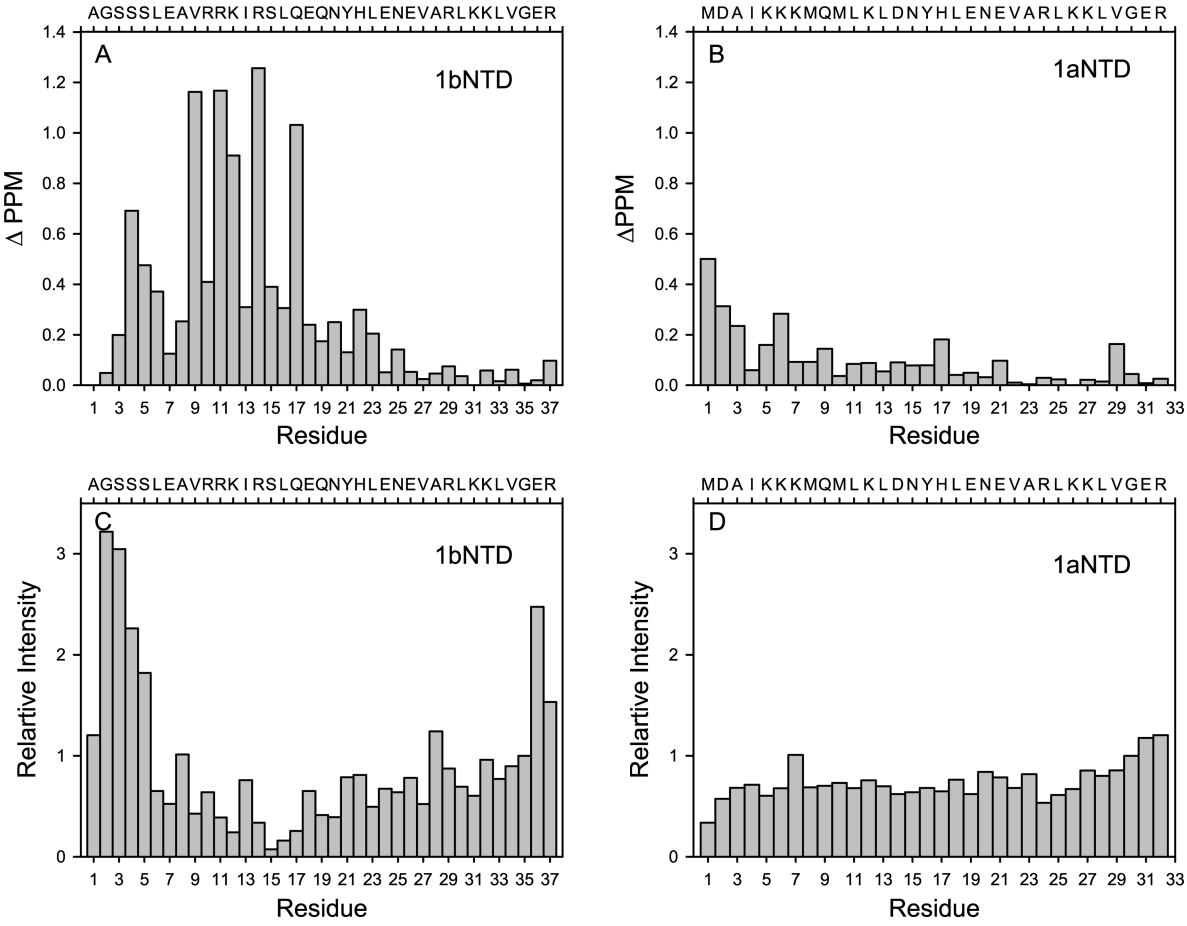

FIGURE 3: Changes in the chemical shifts and relative intensities of the cross-peaks in the $^{15}N-^{1}H$ HSQC spectra of ^{15}N-1bNTD and ^{15}N-1aNTD complexed with unlabeled 9dCTD and 9aCTD, respectively. (A, C) Changes in chemical shifts upon complex formation of the 1b cross-peaks at 20 °C and the 1a cross-peaks at 10 °C, respectively. (B, D) The change in relative intensity upon complex formation of the NH cross-peaks of the 1b and 1a peptides, respectively. The relative intensity changes of the cross-peaks were normalized to the intensities of the cross-peaks of G30 in the 1aNTD spectra and G35 in the 1bNTD spectra, which were set as 1.0. The changes in the intensities of the cross-peaks of 1bNTD upon complex formation suggest that the resonances from residues 12 and 14−17 are broadened due to interaction with residues from the 9dCTD, which are undergoing chemical exchange between multiple conformations. In contrast, there is no evidence of exchange broadening of the cross-peaks in the 1aNTD/9aCTD complex.

shift displacements of 1bNTD in complex with 9dCTD are almost identical to those of the unbound 1bNTD (*9*). There were slight changes in the chemical shifts of two of the $^{13}C^{\alpha}$ resonances, suggesting that S4 and S5 become slightly more helical upon binding, but the rest of the secondary structure is almost unchanged. Residues 6−36 are helical and have coiled-coil interactions as in the free 1bNTD structure (*9*). This indicates that most of the increase in helical content upon complex formation observed using CD (Figure 1) is due to induction of helix in 9dCTD upon binding to 1bNTD.

Tertiary Structure of 1bNTD in the 1bNTD−9dCTD Complex. The structure of 1bNTD in a complex with unlabeled 9dCTD was solved using AutoStructure 1.1.2 (*34, 35*) as described in Materials and Methods. When 1bNTD was bound to 9dCTD, there were no observed intramolecular NOEs between the chains of the bound 1bNTD molecule for residues 1−15, but there were many intermolecular NOEs from the unlabeled 9dCTD to the labeled 1bNTD. The intermolecular CTD to NTD resonances could be uniquely assigned as arising from interactions between the CTD and NTD chains from the X-filtered ^{13}C-edited NOESY spectrum collected when both chains of 1bNTD were labeled and both chains of 9dCTD were unlabeled. The intermolecular NOEs were removed from the data set before the structural calculations were performed. Despite having no intramolecular−interchain NOEs between the chains of the 1bNTD molecule for residues 1−15, there were sufficient intrachain and interchain NOEs from residues 16−37 to define its structure and to determine the conformational changes in the 1bNTD upon binding. Table 2 gives the statistics for the fit of the structure to the NMR data.

In unbound 1bNTD at 8 °C, residues 1−5 are disordered and there are no sequential NOEs from these residues, indicative of a disordered conformation (*9*). In contrast, the NOESY spectra for the 1bNTD in complex with unlabeled 9dCTD at 10 °C showed many NOEs characteristic of α-helices for residues 2−5. There were strong H^{N}_{i} to H^{N}_{i+1} NOEs between G2 and S3, S3 and S4, and S5 and L6, and several H^{α}_{i} to H^{β}_{i+3} and H^{α}_{i} to H^{N}_{i+3} from S4 to E7 and S5 to A8, showing that these residues are ordered when 1bNTD is bound to 9dCTD. We were not able to determine the structure of the bound 1bNTD at 10 °C because the H^{N} resonances from residues 10−16 were too broad due to intermediate chemical exchange to permit assignment of the resonances from the side chains. In addition, there were no unique intramolecular−interchain NOEs arising from residues 1−26 that could be assigned by AutoStructure. At 20 °C the spectra sharpened, and almost all of the resonances

Table 2: Summary of NMR Constraint Data and Structure Quality Statistics for 1bNTD Bound to 9dCTD

NMR Distance and Dihedral Constraints	
Distance Constraints	
total no. of NOE-derived constraints	3276
intraresidue	1544
interresidue	
sequential ($\|i - j\| = 1$)	740
medium range ($1 < \|i - j\| \leq 5$)	864
long-range intrachain ($\|i - j\| > 5$)	0
long-range interchain interactions	128
Hydrogen Bond Constraints	112
Dihedral Angle Restraints	
ϕ	128
χ	128
Constraint Violations (Mean and SD)	0
av no. of distance constraint violations 0.2−0.5 (Å)	0
total no. of close contact violations >0.2 Å	2
Deviations from Idealized Geometry	
bond lengths (Å)	0.007
bond angles (deg)	0.7
impropers (deg)	0
Average Pairwise rmsd (Å)	
all residues, 10 models out of 200	
heavy atoms	2.25
backbone atoms	2.01
helical residues (residues 6−33), 10 models out of 200	
heavy atoms	1.48
backbone atoms	0.87
Ramachandran Plot Summary from Procheck (*62*)	
most favored regions (%)	94.6
additionally allowed regions (%)	4.6
generously allowed regions (%)	0.9
disallowed regions (%)	0.1

	no. of data points	mean parameter value	comparison values: typical value	comparison values: bandwidth	equiv resolution (Å)
Other Plot Statistics from Procheck (*62*)					
H-bond energy SD	10	0.7	1.3	0.2	1.4
χ_1 pooled SD	10	12.7	33.5	4.8	1.3
χ_2 trans SD	10	8.4	31.2	5	1.0

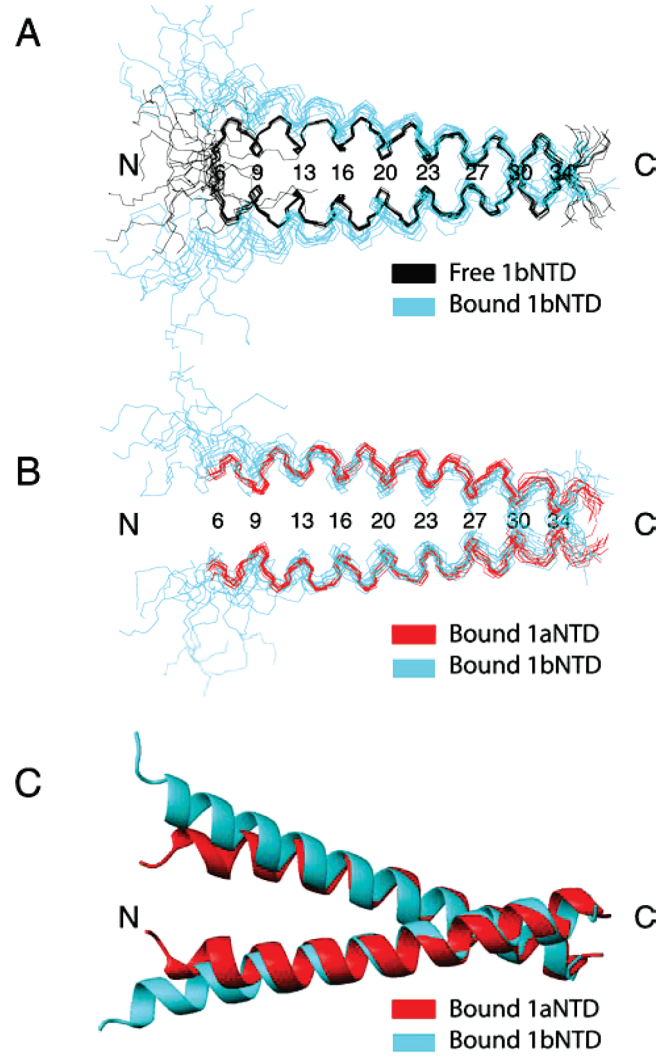

FIGURE 4: Changes in (A) the structure of 1bNTD upon binding to 9dCTD and (B, C) comparison of the bound structure with that of the 1aNTD/9aCTD complex. (A) (black) 1bNTD alone (*9*), RCSB file 1ihq; (cyan) 1bNTD in the 1bNTD/9dNTD complex, RCSB file 2k8x. In unbound 1bNTD residues 1−5 are disordered, and residues 6−19 form a canonical coiled coil, while residues 20−34 from the GCN4 portion of the molecule are also coiled coil. Upon complex formation, residues 4 and 5 become helical, and residues 6−22 splay apart. (B) Backbone structure of (cyan) 1bNTD when complexed to 9dCTD compared to the structure of (red) 1aNTD complexed to 9aCTD. Residues 1−29 of 1aNTD are aligned with the homologous residues 6−34 of 1bNTD. In (A) and (B), the bonds from the peptide backbone are illustrated, and the residues in *a* and *d* positions of the 1bNTD coiled-coil heptad repeat are labeled. (C) Ribbon depictions of the mean backbone structures of the (red) 1aNTD complex compared with the (cyan) 1bNTD complex. The helical residues from the GCN4 portions of the molecules are aligned (residues 15−29 for 1aNTD/9aCTD and 20−34 for the 1bNTD/9dCTD complex). The coordinates of the 1aNTD/9aCTD complex are from the RCSB file 2g9j. The structures of the two NTDs are similar except the helical region of 1bNTD is longer. The figures were drawn using MOLMOL (*64*).

of the molecule could be assigned, allowing determination of the structure, but the H^N_i to H^N_{i+1} NOEs arising from residues 3−5 were broadened. Sequential *i* to *i* + 3 and *i* to *i* + 4 NOEs characteristic of α-helices between residues S4 with E8 and S5 with A8 were observed, suggesting that S4 and S5, which are disordered in the unbound 1bNTD structure, are exchanging between helical and nonhelical conformations at 20 °C.

The backbone structure of 1bNTD bound to 9dCTD is shown in Figure 4A (in cyan) and compared to the free peptide (black). When 1bNTD binds to 9dCTD, residues S4 and S5 become helical and residues 6−18 splay apart to bind to the 9dCTD. The structure of bound 1bNTD is less well defined than free 1bNTD because the intermolecular−interchain NOEs to residues 1−16, needed to constrain the fits of the data, were not identified since the 9dCTD was unlabeled. In addition, some resonances were broadened due to chemical exchange. The N-terminal five residues are probably more ordered than they appear. For example, there were clear intermolecular NOEs to the α-protons of G2 and β-protons of S3 from a leucine methyl group (possibly L274), which would constrain its conformation, but they could not be used in the structure determination since they could not be positively identified. There are numerous intermolecular NOEs to residues 1−16 showing that these residues are making contact at least some of the time when 1bNTD binds to 9dCTD. The refined structure has no upper limit distance constraint violations and no interatomic clashes. The ^{15}N-edited NOESY spectrum suggested that at 10 °C more of the N-terminal extension is helical in the complex, at least transiently, than at 20 °C. Availability of labeled 9dCTD would improve the structure determination of 1bNTD in the complex. We constructed a 9dCTD clone but were unable

to obtain significant expression in *Escherichia coli* under a variety of conditions.

The structure of 1bNTD bound to 9dCTD is similar to that of 1aNTD in complex with 9aCTD, the striated muscle tropomyosin complex (Figure 4B,C). Figure 4B depicts the backbone bonds of 10 structures of 1bNTD (cyan) and 1aNTD (red) where the homologous helical residues are aligned. Figure 4C shows ribbon models of the mean structures aligned by the GCN4 regions of the molecules. The 1bNTD has a longer helical region since S4 and S5, which have no counterparts in 1aNTD, are helical in the complex. The tropomyosin region of the 1bNTD is slightly more splayed than the 1aNTD; the GCN4 portions of the two molecules are almost identical.

Molecular Modeling of the 1bNTD/9dCTD Complex. The intermolecular NOEs between the 9dCTD and 1bNTD gave sufficient information to define the length of the region of the 1bNTD that interacts with the 9dCTD and the residues that are in the intermolecular interface. The experimental data showed that residues G2 to Q17 from the 1bNTD are the binding site for the 9dCTD. (1) The residues of the labeled 1bNTD molecule that have interactions with the unlabeled 9dCTD were identified from their assigned ^{13}C and ^{1}H resonances; there were strong intermolecular NOEs from the 9dCTD to residues G2, S3, L6, A8, V9, and I13 from the1bNTD. (2) The cross-peaks in the $^{1}H-^{15}N$ HSQC spectrum from S4 to L16 of the 1bNTD were greatly shifted upon binding to the 1bCTD. (3) The chemical shifts of the methyl groups from L6, V9 and I13 and L16 were all displaced upon complex formation. (4) The cross-peaks of the amide side chain of Q17 were displaced upon formation of the complex. Since the secondary structure of the 1bNTD was unchanged upon binding, these results provide strong evidence that residues G2−Q17 are all in the intermolecular interface. There was also only one set of NOEs observed for each residue, showing that the complex is symmetric. This finding eliminated a noninterleaved overlap structure.

The structures of bound 1bNTD and bound 1aNTD are similar: the 1bNTD/9dCTD complex is symmetric, and the hydrophobic residues of the 1bNTD with intermolecular NOEs are homologous to the hydrophobic residues of 1aNTD that interact with 9aCTD to form an overlap complex. Based on these findings, the structure of the 1bNTD/9dCTD complex was homology modeled using the coordinates of the NMR structure of the 1aNTD/9aCTD complex (*13*) (see Materials and Methods) (Figure 5). The overall structure of the model of the 1bNTD/9dCTD is similar to that of the solution structure of the 1aNTD/9aCTD complex (*13*). The main difference is that the overlap region in the 1bNTD/9dCTD model is longer than in the 1aNTD/9dCTD complex. Residues 2−17 of 1bNTD interact with residues ∼267−284 from 9dCTD while residues 1−11 of 1aNTD interact with residues 274−284 of 9aCTD in the striated muscle overlap complex.

The interatomic distances <5 Å in the model structure were calculated using MOLMOL. The observed intermolecular NOEs to the 1bNTD are mainly to hydrophobic *a* and *d* residues predicted to be at the NTD/CTD interface: L6, V9, I13, and L16. The observed intermolecular NOEs arising from residues of 1bNTD are consistent with most of the predicted interactions, suggesting that the model is a fair approximation of the actual interface structure and that the

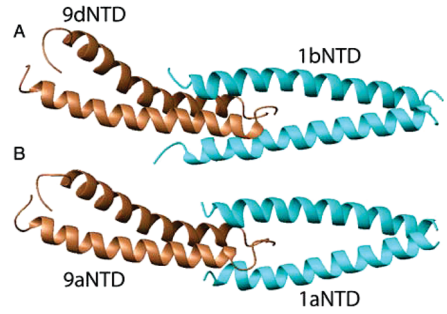

FIGURE 5: Comparison of a model of the 1bNTD/9dCTD complex with the structure of 1aNTD/9aCTD determined by NMR spectroscopy (*13*). The backbones are illustrated by ribbons. (A) Homology model of the 1bNTD/9dCTD complex based on model 1 of the 1aNTD/9aCTD complex, RCSB file 2g9j. (B) 1aNTD/9aCTD. The NTDs are in cyan, and the CTDs are in brown. The overall structures of the complexes are similar, but the overlap region is ∼17 residues compared to ∼11 for the 1aNTD/9aCTD complex. The figures were drawn using MOLMOL (*64*).

nonmuscle overlap region is homologous to the striated muscle overlap complex determined by NMR (*13*). Since the 9dCTD was unlabeled, we evaluated whether the observed intermolecular NOEs from the unlabeled 9dCTD to the labeled 1aNTD were consistent with what would be predicted from the model. The methyl group proton chemical shifts of H^{ε} of Met (∼2.1 ppm), H^{γ} of Thr (∼1.3 ppm), and H^{δ} of Leu (∼0.9 ppm) are distinctive, so some of the 9dCTD *a* and *d* interface residues in the overlap region could be tentatively identified.

Table 3 compares the residues which were predicted to have intermolecular NOEs in the model and the observed NOEs with the observed NOEs in the 1aNTD/9aNTD complex. The model predicts strong interactions of L6 with M273, L274, L278, and T277, A8 with L278 and L279, V9 with L278, L281, and M284, and I13 with L278, L281, and M284. NOEs between resonances of 1bNTD with resonances having chemical shifts consistent with these interactions were observed.

The major differences between the predicted and observed NOEs in our model were in the N-terminal extension, A1−S5, that vary in conformation among the ten NMR models (Figure 5A); we did not include these interactions in Table 3. Some of the predicted interactions were not observed, and interactions between S3 and a leucine residue (L274 or L278) were observed that were not predicted. The major differences were that predicted interactions of L16 with M284 as well as extensive predicted interactions with K12 were not observed. Intramolecular cross-peaks from the side chains of these two residues in the NOESY spectra were weak, suggesting these residues undergo exchange broadening at 20 °C. The cross-peaks from both of these residues, however, were displaced from those of the unbound 1bNTD, suggesting they do indeed form part of the 1bNTD/9dCTD interface. Predicted NOEs between resonances of V9 with T277 were also not observed, possibly because T277 in 9dCTD is less hydrophobic than A277 in 9aCTD.

While the pattern of NOEs in the 1bNTD/9dCTD complex is consistent with major interactions between L6−L16 and residues 274−284 of the 9dCTD (homologous to the structure of the 1aNTD/9aNTD overlap complex), L6 to L16 would have a similar pattern of NOEs if L6 were aligned with T277 rather than L274. Both models have a similar

Table 3: Intermolecular NOEs Consistent with the Model of the 1bNTD/9dCTD Complex

residue	consistent predicted NOEs	predicted NOEs not observed	homologous residue in 1aNTD/9aCTD complex	observed NOEs in 1aNTD/9aCTD complex
L6	M273, L274 and/or L278, T277		M1	I270, E273, L274, A277, L278
A8	L278		A3	L278
V9	L278 and/or L281, M284	T277	I4	L278, M281, I284
R10	L281, E280	T277	K5	A277, L278, M281, I284
K12[a]	M284	L278, N282	K7	M281, T282, I284
I13	L278 and/or L281, M284		M8	M281, I284
L16[a]		M284	L11	M281, I284
Q17[b]	L281, M284		K12	I284

[a] Cross-peaks from K12 and L16 were broadened upon complex formation. [b] The cross-peaks from the side-chain amides of Q17 were shifted upon complex formation.

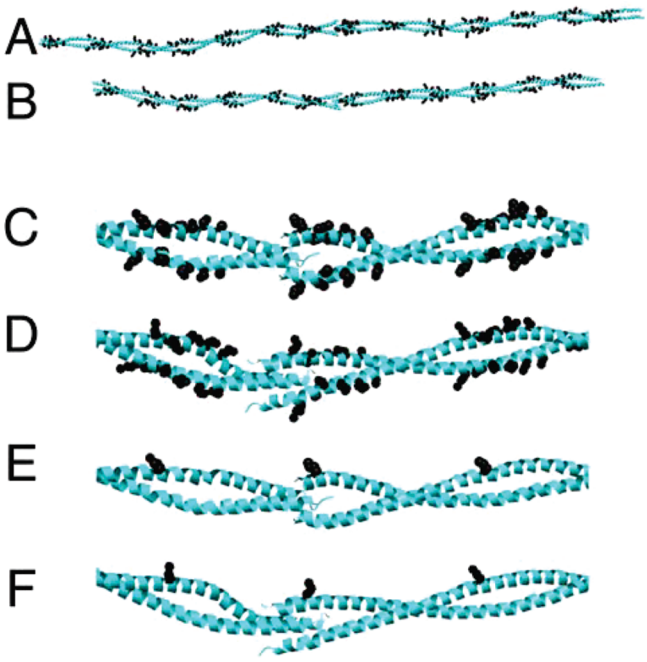

FIGURE 6: Models of full-length striated and nonmuscle tropomyosin molecules associated head to tail. (A) Two molecules from the 7 Å structure of striated muscle TM (*38*) linked via one model structure of the NMR ensemble of the 1aNTD/9aCTD complex (*13*). The model is shown in ribbon format (cyan) with the side chains (carbon atoms) of "consensus residues" in each of the seven proposed actin binding sites shown in spheres (black). The "consensus" residues are a repeated motif of seven polar and nonpolar surface residues that have the periodicity and spacing to be actin binding sites (*14*). Mutagenesis experiments have shown that they are required for tropomyosin to bind to F-actin (*51*). (B) Model of two molecules of LMW α-tropomyosin linked by the 1bNTD/9dCTD complex. (C, D) Details of three sequential proposed actin binding sites including the one in the intermolecular junction. (C) 1aNTD/9aCTD. (D) 1bNTD/9dCTD. (E, F) Views of the junctional regions of the 1aNTD/9aCTD model (E) and the 1bNTD/9dCTD model (F) highlighting (in black) single side chains of the first residue from consensus sites 7, 1, and 2 in the 1aNTD/9aCTD complex and sites 6, 1, and 2 in the 1bNTD/9dCTD complex. The side chains are shown on one side of each coiled coil. In the 1aNTD/9aCTD complex they are R244, K6, and K48, respectively, showing their similar orientations. In the 1bNTD/9dCTD short tropomyosin complex, the homologous residues are R207, R11, and R53. The models show that the consensus residues' side chains of the three sequential periods have similar orientations relative to the axis of the coiled coil. In both models, the planes of the N termini relative to the planes of the C termini are rotated by 90°. As a result, the orientation of the proposed consensus residues (shown in black) of the actin binding sites on the surface is retained from one molecule to the next along the filament. The figures were drawn using UCSF-Chimera (*65*).

spectrum of predicted NOEs, although the relative intensities of the various peaks would be different. The pattern of NOEs, however, is inconsistent with L6 being aligned with N267, M270, or M281. The correct alignment must await determination of the full structure. We have elected to show the model with the longer overlap region since it incorporates the sequence homology between 1aNTD and 1bNTD.

The solution structures of 1bNTD in the complex and the striated muscle overlap complex are not similar to the crystal structure of the striated muscle overlap complex (RCSB 2z5i (*43*),) in which one molecule of an N-terminal TM model peptide dimer interacts with two molecules of a C-terminal TM model peptide dimer. The extensive hydrophobic intermolecular interactions of L6 and I13 with the 9dCTD and observed intermolecular NOEs from the 9dCTD to resonances from the side chains of R10 are incompatible with the 1bNTD/9dCTD complex having such a structure.

DISCUSSION

A distinguishing characteristic of LMW tropomyosins expressed in nonmuscle cells, in addition to being shorter, is the presence of an N-terminal extension of five residues in mammalian tropomyosins that is disordered in solution (*9*). When an N-terminal model peptide, 1bNTD, binds to a C-terminal peptide, 9dCTD, the extension becomes more helical. Residues 2−5, along with the following 11 residues, are engaged in binding that also induces helical formation of 9dCTD. The homologous regions of both HMW and LMW N-terminal domains have similar coiled-coil structures.

A homology model of the LMW intermolecular overlap complex was constructed using the coordinates of the HMW striated muscle complex (*13*), initially based on sequence homology and supported by NMR data. The structures of the two complexes are similar overall in being symmetric and in the perpendicular orientation of the planes of the coiled coils in the complex. The major difference is that the overlap region of the LMW complex is 16 residues, compared to 11 for the HMW complex because of the involvement of the N-terminal extension. Second, although the affinity of the LMW ends for each other is higher than that of the HMW ends, at physiological temperature much of the C-terminal region is disordered and exchanges between ordered and disordered states. That is, the unfolding of the complex is uncoupled from dissociation, in contrast to other complexes we have studied.

A major outcome of the solution structure of the striated muscle tropomyosin junctional complex is the insight gained into how the proposed periodic actin binding sites on

tropomyosin relate to the actin subunits in the actin filament (*14*). The 7-fold periodicity in the striated muscle tropomyosin sequence was recognized when the sequence became available (*14, 44, 45*). The pitch of the supercoil is variable along the length of the molecule (*38*), and one might intuitively expect there to be seven half-turns of the supercoil per molecule that correspond to the seven actin subunits along the length of one HMW tropomyosin molecule. Our analysis of the 7 Å structure using TWISTER (*46*) showed there are only ~5.75 half-turns of the supercoil (*13*). The perpendicular orientation of the planes of the coiled coils of the molecules that form the complex "corrects" for the quarter turn. Modeling of tropomyosin molecules joined by the overlap complex on the actin filament showed that the proposed actin binding sites from one tropomyosin molecule to the next present a similar face to the actin subunits, even though the repeats do not correspond to supercoil repeats. Were the planes parallel, as in earlier models (*47, 48*), this would not be the case.

Does the longer N terminus of LMW tropomyosin change the alignment of the proposed actin binding sites with respect to the actin filament? To address this question we modeled the LMW overlap complex into the striated muscle tropomyosin structure (see Materials and Methods; compare panels A and B of Figure 6). The arrangement of the surface residues in tropomyosin with the LMW junction is comparable to that with the HMW forms (compare panels C and E of Figure 6 with panels D and F of Figure 6, respectively).

We have considered how the recombinant LMW α-tropomyosins have higher actin affinity than HMW α-tropomyosins even though there are six versus seven postulated actin binding sites. Both circular dichroism and NMR data show that although the ends encoded by exon 1b and exon 9d form a tight intermolecular junction, the overlap region is relatively disordered and undergoes chemical exchange between multiple conformations. Conformational flexibility (instability) is essential for formation of the 1aNTD/9aCTD complex and for troponin T binding (*49*) as well as for the binding of tropomyosin to actin (*50, 51*). The disordered 9d C terminus may facilitate strong actin binding (*5, 52*) since the instability gives the conformational freedom to find the correct binding partners. We also suggest that the longer N-terminal region encoded by exon 1b contributes to the greater actin affinity of recombinant LMW rat α-tropomyosins (*5*) and the influence of the N terminus on the regulatory state of the actin filament (*53*). Support for the idea that the N-terminal region (AGSSSLEAVRRKIR) may encode an actin binding site is its homology to an internal cofilin sequence (rat cofilin residues 114−127, IYASSKDAIKKKLT) that is helical in solution (*54*) and in X-ray structures of yeast and bovine cofilins (*55*). The region is part of and/or close to an actin binding site on cofilin (*56*−*58*). Cofilin binds with high affinity to the actin filament. Tropomyosin is a competitive inhibitor of cofilin binding and severing (*59*−*61*). Tropomyosin's ability to inhibit cofilin binding and severing may reflect direct competition for binding sites on the actin filament, as well as its generic ability to stabilize the actin filament against severing proteins.

ACKNOWLEDGMENT

We thank Brian Rapp for assistance in peptide expression and purification, Dr. T. Swapna for expertise in collection of the NMR spectra, and Dr. Guy Montelione for continued support of the project.

SUPPORTING INFORMATION AVAILABLE

A figure and experimental details showing the binding of 1aNTD and 1bNTD with two 39-residue peptides containing the C termini of rat tropomyosins encoded by exon 9a (9a39) and exon 9d (9d39), respectively, and the coordinates of the model of the 1bNTD/9dCTD complex shown in Figure 5A in pdb format. This material is available free of charge via the Internet at http://pubs.acs.org.

REFERENCES

1. Gunning, P., O'Neill, G., and Hardeman, E. (2008) Tropomyosin-based regulation of the actin cytoskeleton in time and space. *Physiol. Rev. 88*, 1–35.
2. Kostyukova, A. S., Hitchcock-Degregori, S. E., and Greenfield, N. J. (2007) Molecular basis of tropomyosin binding to tropomodulin, an actin-capping protein. *J. Mol. Biol. 372*, 608–618.
3. Kostyukova, A. S. (2008) Tropomodulins and tropomodulin/tropomyosin interactions. *Cell. Mol. Life Sci. 65*, 563–569.
4. Brown, J. H., and Cohen, C. (2005) Regulation of muscle contraction by tropomyosin and troponin: how structure illuminates function. *Adv. Protein Chem. 71*, 121–159.
5. Moraczewska, J., Nicholson-Flynn, K., and Hitchcock-DeGregori, S. E. (1999) The ends of tropomyosin are major determinants of actin affinity and myosin subfragment 1-induced binding to F-actin in the open state. *Biochemistry 38*, 15885–15892.
6. Palm, T., Greenfield, N. J., and Hitchcock-DeGregori, S. E. (2003) Tropomyosin ends determine the stability and functionality of overlap and troponin T complexes. *Biophys. J. 84*, 3181–3189.
7. Greenfield, N. J., Montelione, G. T., Farid, R. S., and Hitchcock-DeGregori, S. E. (1998) The structure of the N-terminus of striated muscle alpha-tropomyosin in a chimeric peptide: nuclear magnetic resonance structure and circular dichroism studies. *Biochemistry 37*, 7834–7843.
8. Brown, J. H., Kim, K. H., Jun, G., Greenfield, N. J., Dominguez, R., Volkmann, N., Hitchcock-DeGregori, S. E., and Cohen, C. (2001) Deciphering the design of the tropomyosin molecule. *Proc. Natl. Acad. Sci. U.S.A. 98*, 8496–8501.
9. Greenfield, N. J., Huang, Y. J., Palm, T., Swapna, G. V., Monleon, D., Montelione, G. T., and Hitchcock-DeGregori, S. E. (2001) Solution NMR structure and folding dynamics of the N terminus of a rat non-muscle alpha-tropomyosin in an engineered chimeric protein. *J. Mol. Biol. 312*, 833–847.
10. Li, Y., Mui, S., Brown, J. H., Strand, J., Reshetnikova, L., Tobacman, L. S., and Cohen, C. (2002) The crystal structure of the C-terminal fragment of striated-muscle alpha-tropomyosin reveals a key troponin T recognition site. *Proc. Natl. Acad. Sci. U.S.A. 99*, 7378–7383.
11. Greenfield, N. J., Swapna, G. V., Huang, Y., Palm, T., Graboski, S., Montelione, G. T., and Hitchcock-DeGregori, S. E. (2003) The structure of the carboxyl terminus of striated alpha-tropomyosin in solution reveals an unusual parallel arrangement of interacting alpha-helices. *Biochemistry 42*, 614–619.
12. Nitanai, Y., Minakata, S., Maeda, K., Oda, N., and Maeda, Y. (2007) Crystal structures of tropomyosin: flexible coiled-coil. *Adv. Exp. Med. Biol. 592*, 137–151.
13. Greenfield, N. J., Huang, Y. J., Swapna, G. V., Bhattacharya, A., Rapp, B., Singh, A., Montelione, G. T., and Hitchcock-Degregori, S. E. (2006) Solution NMR structure of the junction between tropomyosin molecules: implications for actin binding and regulation. *J. Mol. Biol. 364*, 80–96.
14. Phillips, G. N., Jr. (1986) Construction of an atomic model for tropomyosin and implications for interactions with actin. *J. Mol. Biol. 192*, 128–131.
15. Ozeki, S., Kato, T., Holtzer, M. E., and Holtzer, A. (1991) The kinetics of chain exchange in two-chain coiled coils: alpha alpha- and beta beta-tropomyosin. *Biopolymers 31*, 957–966.
16. Goa, J. (1953) A micro biuret method for protein determination. *Scand. J. Clin. Lab. Invest. 5*, 218–222.

17. Greenfield, N. J. (2006) Using circular dichroism, collected as a function of temperature, to determine the thermodynamics of protein folding and binding interactions. *Nat. Protocols 1*, 2527–2535.
18. Bohm, G., Muhr, R., and Jaenicke, R. (1992) Quantitative analysis of protein far UV circular dichroism spectra by neural networks. *Protein Eng. 5*, 191–195.
19. Greenfield, N. J. (2006) Determination of the folding of proteins as a function of denaturants, osmolytes or ligands using circular dichroism. *Nat. Protocols 1*, 2733–2741.
20. Engel, G. (1974) Estimation of binding parameters of enzyme-ligand complex from fluorometric data by a curve fitting procedure: seryl-tRNA synthetase- tRNA Ser complex. *Anal. Biochem. 61*, 184–191.
21. Marquardt, D. W. (1963) An algorithm for the estimation of non-linear parameters. *J. Soc. Indust. Appl. Math. 11*, 431–441.
22. Bodenhausen, G., and Ruben, D. J. (1980) Natural abundance nitrogen-15 NMR by enhanced heteronuclear spectroscopy. *Chem. Phys. Lett. 69*, 185–189.
23. Kay, L. E., Keifer, P., and Saarinen, T. (1992) Pure absorption gradient enhanced heteronuclear single quantum correlation spectroscopy with improved sensitivity. *J. Am. Chem. Soc. 114*, 10663–10665.
24. Muhandiram, D. R., and Kay, L. E. (1994) Gradient-enhanced triple-resonance three-dimensional NMR experiments with improved sensitivity. *J. Magn. Reson., Ser. B 103*, 203–216.
25. Boucher, W., Laue, E. D., Campbell-Burk, S. L., and Domaille, P. J. (1991) Four dimensional heteronuclear triple resonance NMR methods for the assignment of backbone nuclei in proteins. *J. Am. Chem. Soc. 114*, 2262–2264.
26. Feng, W., Rios, C. B., and Montelione, G. T. (1996) Phase labeling of C-H and C-C spin-system topologies: application in PFG-HACANH and PFG-HACA(CO)NH triple-resonance experiments for determining backbone resonance assignments in proteins. *J. Biomol. NMR 8*, 98–104.
27. Rios, C. B., Feng, W., Tashiro, M., Shang, Z., and Montelione, G. T. (1996) Phase labeling of C-H and C-C spin-system topologies: application in constant-time PFG-CBCA(CO)NH experiments for discriminating amino acid spin-system types. *J. Biomol. NMR 8*, 345–350.
28. Grzesiek, S., and Bax, A. (1993) Amino acid type determination in the sequential assignment procedure of uniformly $^{13}C/^{15}N$-enriched proteins. *J. Biomol. NMR 3*, 185–204.
29. Kay, L. E., Ikura, M., and Bax, A. (1990) Proton proton correlation via carbon-carbon couplings. A three dimensional NMR approach for the assignment of aliphatic resonances in proteins labeled with C-13. *J. Am. Chem. Soc. 112*, 888–889.
30. Bax, A., Clore, G. M., and Gronenborn, A. M. (1990) ^{1}H-^{1}H correlation via isotropic mixing of ^{13}C magnetization, a new three-dimensional approach for assigning ^{1}H and ^{13}C spectra of ^{13}C enriched proteins. *J. Magn. Reson. 88*, 425–431.
31. Driscoll, P. C., Clore, G. M., Marion, D., Wingfield, P. T., and Gronenborn, A. M. (1990) Complete resonance assignment for the polypeptide backbone of interleukin 1 using three-dimensional heteronuclear NMR spectroscopy. *Biochemistry 29*, 3542–3556.
32. Ikura, M., Kay, L. E., and Bax, A. (1990) A novel approach for sequential assignment of ^{1}H, ^{13}C, and ^{15}N spectra of proteins: heteronuclear triple-resonance three-dimensional NMR spectroscopy. Application to calmodulin. *Biochemistry 29*, 4659–4667.
33. Zwahlen, C., Legault, P., Vincent, S. J. F., Grdenblatt, J., Konrat, R., and Kay, L. E. (1997) Methods for measurement of intermolecular NOEs by multinuclear NMR spectroscopy: application to a bacteriophage 107 N-peptide/boxB RNA complex. *J. Am. Chem. Soc. 119*, 6711–6721.
34. Huang, Y. J. (2001) Automated determination of protein structures from NMR data by iterative analysis of self-consistent contact patterns, Ph.D. Thesis, Rutgers University, New Brunswick, NJ.
35. Huang, Y. J., Moseley, H. N., Baran, M. C., Arrowsmith, C., Powers, R., Tejero, R., Szyperski, T., and Montelione, G. T. (2005) An integrated platform for automated analysis of protein NMR structures. *Methods Enzymol. 394*, 111–141.
36. Güntert, P., Mumenthaler, C., and Wüthrich, K. (1997) Torsion angle dynamics for NMR structure calculation with the new program DYANA. *J. Mol. Biol. 273*, 283–298.
37. Brunger, A. T., Adams, P. D., Clore, G. M., DeLano, W. L., Gros, P., Grosse-Kunstleve, R. W., Jiang, J. S., Kuszewski, J., Nilges, M., Pannu, N. S., Read, R. J., Rice, L. M., Simonson, T., and Warren, G. L. (1998) Crystallography & NMR system: A new software suite for macromolecular structure determination. *Acta Crystallogr., Sect. D: Biol. Crystallogr. 54* (Part 5), 905–921.
38. Whitby, F. G., and Phillips, G. N., Jr. (2000) Crystal structure of tropomyosin at 7 angstroms resolution. *Proteins 38*, 49–59.
39. Goodwin, L. O., Lees-Miller, J. P., Leonard, M. A., Cheley, S. B., and Helfman, D. M. (1991) Four fibroblast tropomyosin isoforms are expressed from the rat alpha-tropomyosin gene via alternative RNA splicing and the use of two promoters. *J. Biol. Chem. 266*, 8408–8415.
40. Jancso, A., and Graceffa, P. (1991) Smooth muscle tropomyosin coiled-coil dimers. Subunit composition, assembly, and end-to-end interaction. *J. Biol. Chem. 266*, 5891–5897.
41. Greenfield, N. J., and Hitchcock-DeGregori, S. E. (1995) The stability of tropomyosin, a two-stranded coiled-coil protein, is primarily a function of the hydrophobicity of residues at the helix-helix interface. *Biochemistry 34*, 16797–16805.
42. Kremneva, E., Nikolaeva, O., Maytum, R., Arutyunyan, A. M., Kleimenov, S. Y., Geeves, M. A., and Levitsky, D. I. (2006) Thermal unfolding of smooth muscle and nonmuscle tropomyosin alpha-homodimers with alternatively spliced exons. *FEBS J. 273*, 588–600.
43. Murakami, K., Stewart, M., Nozawa, K., Tomii, K., Kudou, N., Igarashi, N., Shirakihara, Y., Wakatsuki, S., Yasunaga, T., and Wakabayashi, T. (2008) Structural basis for tropomyosin overlap in thin (actin) filaments and the generation of a molecular swivel by troponin-T. *Proc. Natl. Acad. Sci. U.S.A. 105*, 7200–7205.
44. Parry, D. A. (1975) Analysis of the primary sequence of alpha-tropomyosin from rabbit skeletal muscle. *J. Mol. Biol. 98*, 519–535.
45. McLachlan, A. D., and Stewart, M. (1976) The 14-fold periodicity in tropomyosin and the interaction with actin. *J. Mol. Biol. 103*, 271–298.
46. Strelkov, S. V., and Burkhard, P. (2002) Analysis of α-helical coiled coils with the program TWISTER reveals a structural mechanism for stutter compensation. *J. Struct. Biol. 137*, 54–64.
47. McLachlan, A. D., and Stewart, M. (1975) Tropomyosin coiled-coil interactions: evidence for an unstaggered structure. *J. Mol. Biol. 98*, 293–304.
48. Lorenz, M., Poole, K. J., Popp, D., Rosenbaum, G., and Holmes, K. C. (1995) An atomic model of the unregulated thin filament obtained by X-ray fiber diffraction on oriented actin-tropomyosin gels. *J. Mol. Biol. 246*, 108–119.
49. Greenfield, N. J., Palm, T., and Hitchcock-DeGregori, S. E. (2002) Structure and interactions of the carboxyl terminus of striated muscle alpha-tropomyosin: it is important to be flexible. *Biophys. J. 83*, 2754–2766.
50. Singh, A., and Hitchcock-DeGregori, S. E. (2003) Local destabilization of the tropomyosin coiled coil gives the molecular flexibility required for actin binding. *Biochemistry 42*, 14114–14121.
51. Singh, A., and Hitchcock-DeGregori, S. E. (2006) Dual requirement for flexibility and specificity for binding of the coiled-coil tropomyosin to its target, actin. *Structure 14*, 43–50.
52. Cho, Y. J., and Hitchcock-DeGregori, S. E. (1991) Relationship between alternatively spliced exons and functional domains in tropomyosin. *Proc. Natl. Acad. Sci. U.S.A. 88*, 10153–10157.
53. Maytum, R., Lehrer, S. S., and Geeves, M. A. (1999) Cooperativity and switching within the three-state model of muscle regulation. *Biochemistry 38*, 1102–1110.
54. Pope, B. J., Zierler-Gould, K. M., Kuhne, R., Weeds, A. G., and Ball, L. J. (2004) Solution structure of human cofilin: actin binding, pH sensitivity, and relationship to actin-depolymerizing factor. *J. Biol. Chem. 279*, 4840–4848.
55. Fedorov, A. A., Lappalainen, P., Fedorov, E. V., Drubin, D. G., and Almo, S. C. (1997) Structure determination of yeast cofilin. *Nat. Struct. Biol. 4*, 366–369.
56. Lappalainen, P., Fedorov, E. V., Fedorov, A. A., Almo, S. C., and Drubin, D. G. (1997) Essential functions and actin-binding surfaces of yeast cofilin revealed by systematic mutagenesis. *EMBO J. 16*, 5520–5530.
57. Guan, J. Q., Vorobiev, S., Almo, S. C., and Chance, M. R. (2002) Mapping the G-actin binding surface of cofilin using synchrotron protein footprinting. *Biochemistry 41*, 5765–5775.
58. Moriyama, K., and Yahara, I. (2002) The actin-severing activity of cofilin is exerted by the interplay of three distinct sites on cofilin and essential for cell viability. *Biochem. J. 365*, 147–155.
59. Bernstein, B. W., and Bamburg, J. R. (1982) Tropomyosin binding to F-actin protects the F-actin from disassembly by brain actin-depolymerizing factor (ADF). *Cell Motil. 2*, 1–8.

60. Nishida, E., Maekawa, S., and Sakai, H. (1984) Cofilin, a protein in porcine brain that binds to actin filaments and inhibits their interactions with myosin and tropomyosin. *Biochemistry 23*, 5307–5313.
61. DesMarais, V., Ichetovkin, I., Condeelis, J., and Hitchcock-DeGregori, S. E. (2002) Spatial regulation of actin dynamics: a tropomyosin-free, actin-rich compartment at the leading edge. *J. Cell Sci 115*, 4649–4660.
62. Laskowski, R. A., Rullmannn, J. A., MacArthur, M. W., Kaptein, R., and Thornton, J. M. (1996) AQUA and PROCHECK-NMR: programs for checking the quality of protein structures solved by NMR. *J. Biomol. NMR 8*, 477–486.
63. Savitsky, A., and Golay, M. J. E. (1964) Smoothing and dIfferentiation of data by simplified least squares procedures. *Anal. Chem. 36*, 1627–1639.
64. Koradi, R., Billeter, M., and Wüthrich, K. (1996) MOLMOL: a program for display and analysis of macromolecular structures. *J. Mol. Graphics 14*, 51–55.
65. Pettersen, E. F., Goddard, T. D., Huang, C. C., Couch, G. S., Greenblatt, D. M., Meng, E. C., and Ferrin, T. E. (2004) UCSF Chimera—a visualization system for exploratory research and analysis. *J. Comput. Chem. 25*, 1605–1612.

BI801861K